THE JOURNAL OF PHYSICAL CHEMISTRY C

Article

pubs.acs.org/JPCC

Nucleation of Methane Hydrates at Moderate Subcooling by Molecular Dynamics Simulations

Felipe Jiménez-Ángeles[†] and Abbas Firoozabadi*[,†,‡]

[†]Reservoir Engineering Research Institute, Palo Alto, California 94301, United States

[‡]Department of Chemical and Environmental Engineering, Yale University, New Haven, Connecticut 06510, United States

Supporting Information

ABSTRACT: Methane hydrates are crystalline structures composed of cages of hydrogen-bonded water molecules in which methane molecules are trapped. The nucleation mechanisms of crystallization are not fully resolved, as they cannot be accessed experimentally. For methane hydrates most of the reported simulations on the phenomena capture some of the basic elements of the full structure. In few reports, formation of crystalline structures is reached by imposing very high pressure, or dynamic changes of temperature, or a pre-existing hydrate structure. In a series of nanoscale molecular dynamics simulations of supersaturated water−methane mixtures, we find that the order of the crystalline structure increases by decreasing subcooling. Crystalline structures I and II form and coexist at moderate temperatures. Crystallization initiates from the spontaneous formation of an amorphous cluster wherein structures I, II, and other ordered defects emerge. We observe the transient coexistence of sI and sII in agreement with experiments. Our simulations are carried out at high methane supersaturation. This condition dramatically reduces the nucleation time and allows simulating nucleation at moderate subcooling. Moderate temperatures drive hydrates to more ordered structures.

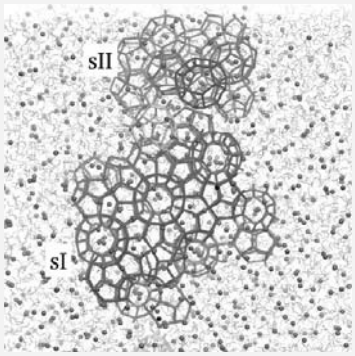

INTRODUCTION

At low temperature and moderate pressure a mixture of water and methane and other small molecules may form an ice-like phase known as clathrate hydrates. These are crystalline structures of water-forming cages in which small molecules known as guest molecules stabilize the cage.[1,2] The ratio of guest to water molecules can be up to 0.15 when all the cavities are filled. Typical guest molecules include methane, ethane, CO_2, and ethylene oxide.[3] Hydrates have a broad range of technological applications including separation and sequestration processes, fuel transportation, climate change, hydrogen storage, geology, planetary and marine sciences, and so on.[4−10] Large reserves of methane hydrate exist under the sediments of the ocean floors making it the most abundant clathrate hydrate and an important source of hydrocarbon energy.[11−13] Hydrates may also cause serious safety and environmental concern in hydrocarbon production.[14] The capture of oil in the recent accident in the Gulf of Mexico was unsuccessful because of formation of hydrates.[15]

Methane hydrates form when water and methane are brought into contact at hydrate formation conditions (T, P). At those conditions both components (mixed and separated) may stay for a long period at a metastable fluid state. The equilibrium state includes the methane hydrate solid. Formation of hydrates requires the dissolution of methane in water. At some time hydrates nucleate and start to grow. In experimental setups consisting of methane gas and water, a reservoir of methane is required to maintain the pressure constant. The consumption of methane means that it is dissolved into water. During the growth stage methane is incorporated into the cages of the hydrate structure. The induction time is defined when hydrates become detectable macroscopically (typically between few minutes up to days). An equivalent way to define the induction time is when a detectable consumption of methane starts. The nucleation time refers to the formation of the first stable hydrate nucleus. It can not be determined with precision due to the difficulty to detect hydrates nuclei.

According to nucleation theory, it is necessary to overcame a Gibbs free energy barrier to form methane hydrate from an unstable state.[16,17] The magnitude of the Gibbs free energy barrier is given by the energy needed to create a crystal−fluid interface plus the energy gain to create the crystal volume. The driving force to overcome the free energy barrier is the difference between the chemical potentials of the old and new phases.[18] Low temperature, high pressure, and high supersaturation (excess of methane in the solution) increase the driving force and prompt hydrate formation. In nucleation theory the nucleation time is a strong function of supersaturation. By increasing supersaturation the nucleation time decreases.[16]

The molecular mechanism of hydrate nucleation is a fundamental open question. Molecular simulations have been used to uncover some of the molecular mechanisms of nucleation and growth of clathrate hydrates. Rodger et

Received: January 8, 2014
Revised: May 5, 2014
Published: May 6, 2014

al.[19−21] simulate an interface of methane gas next to a water−methane solution. Their setup is constructed by melting a methane hydrate crystal at high temperature. While the aqueous solution is metaestable (supersaturated) the system is carried to hydrate formation conditions. They observe formation of hydrate structures within the first 5 ns of simulation. Walsh et al.[22,23] construct a methane gas−aqueous solution interface equilibrated at high temperature. The concentration of methane in the aqueous solution is very low as a consequence of the equilibration process. In a second step the setup is brought to hydrate formation conditions. Prior to hydrate nucleation the number of methane molecules dissolved in the aqueous solution increases significantly. Depending on the simulation conditions (T, P), the simulation times to observe formation of stable hydrate structures range from several hundreds of nanoseconds up to several microseconds. Using a similar arrangement and a coarse grain model of water, Jacobson et al.[24,25] study hydrate formation of methane, carbon dioxide, and generic guests. Liang and Kusalik explore nucleation of H_2S in a related setup.[26]

A common condition of the studies on hydrate nucleation mentioned above is that hydrate formation is triggered when methane concentration in the aqueous solution is above certain minimal value.[27] In a detailed study, Walsh et al. quantify the methane mole fraction dissolved in water at the instant of nucleation. They find a strong dependence with temperature, pressure, and the geometry of the interface. At prenucleation conditions, the methane mole fraction ranges from 0.02 up to 0.04, for temperatures between 245−250 K and pressures between 50−4000 bar.[28] Guo and Rodger find a critical value of the methane mole fraction around 0.05 beyond which hydrate structures spontaneously form.[29] A mole fraction of up to 0.077 has been detected in nucleation of H_2S hydrates.[26] For H_2S the equilibrium solubility in water is high and the melting temperature of the H_2S hydrtae is higher than for the methane hydrate.

Subcooling is defined as $\Delta T_s = T_m - T$, where T_m is the melting temperature and T is the temperature of the system. A common consideration in the studies addressing hydrate nucleation is a high subcooling ($\Delta T_s \geq 50$ K) and high pressure. In molecular simulations of hydrates the melting temperature depends on the models of water and guest molecules. A water model that better describes the ice temperature is also expected to describe well the hydrate melting temperature.[30] Increasing subcooling and the pressure increase methane solubility in water which in turn increases the probability to form stable hydrate cages.[29−31] In order to produce hydrate structures in reasonable computational times, simulation studies are carried out at high pressures and high subcoolings.[19−24,28] The drawback of such considerations is that the systems are driven into arrested states. In general, structures with long-range order are not formed; amorphous clusters containing structural units of clathrate hydrates (cages from sI, sII, and other type of cages)[19−22,24,32−34] are formed. The formation of sI is observed at very high pressure (200 MPa) and low temperature (T = 245−250 K).[23] A continuous increase of temperature in NVE simulations of H_2S solutions gives rise to structures with relatively high crystalline order.[35]

In a recent approach Sarupria and Debeneditti suggest a supersaturated homogeneous mixture of dissolved gas in water[36] with 0.07 methane mole fraction at T = 240 K and P = 20 MPa. By doing so, they observe formation of hydrate clusters over time scales of several hundreds of nanoseconds. The structures are similar to those found in two-phase simulation setups at high subcooling.[19−24,28]

A number of authors consider a pre-existing hydrate structure to study hydrate growth.[33,34,37−39] This approach allows studying crystal growth but leaves out the fundamentals of initial stages of the nucleus formation. Crystalline hydrate phases sI and sII may grow from an amorphous cluster at moderate subcooling.[39] Based on this observation, a two-step scheme[24,34] in crystal nucleation has been proposed consisting of (1) the initial formation of amorphous clusters and (2) the evolution of clusters toward a crystalline state at macroscopic times. The simulation time to observe the second step at the temperatures at which the amorphous clusters are nucleated is beyond the simulation time scale.

Despite major efforts in simulation addressing hydrate nucleation, the underlying mechanism of the formation of crystal structures is not yet fully clear. Several investigations indicate that temperature has an important effect on the order of the crystalline structure.[24,34,35] To the best of our knowledge, the initial stages of methane hydrate nucleation have not been studied nor the full process from spontaneous nucleation and crystal growth at moderate subcooling. In this work we carry out molecular dynamics simulations of supersaturated homogeneous mixtures of methane and water at moderate temperatures. Methane concentration is set by our design beyond the limit of equilibrium solubility. By doing so, hydrates form without a high subcooling. Large methane concentration allows to observe some of the underlying mechanisms of crystal nucleation in accessible computational times. Moderate temperatures aid the formation of the crystalline hydrate structures.

■ MODELS AND SIMULATION METHOD

A homogeneous mixture of methane and water is constructed by placing randomly N_m methane molecules and N_w water molecules into a cubic L-side box. The initial box size is calculated based on a total density of the mixture around 0.67 g/cm^3. The overlapping positions of particles at the initial configuration are prevented by distance and energy criteria. A 3 ns simulation is carried out to stabilize the system at the target temperature T and pressure P. The stabilization run is carried out at the same conditions as the production run. During the stabilization simulation, the volume of the cell decreases about 20%. The resulting configuration is the initial of a molecular dynamics simulation of several hundreds of nanoseconds which is monitored for hydrate formation. We select a pressure of 50 MPa and temperatures from 250 to 285 K corresponding to subcooling of 54 K $\gtrsim \Delta T_s \gtrsim$ 19 K (the melting temperature of the hydrate estimated by molecular dyanamics simulations[30,40] is ∼304 K at P = 50 MPa). A summary of the simulation conditions is given in Table 1.

Water molecules are modeled by the TIP4P-ice[41] while methane molecules are described as spherical particles. The Lennard-Jones parameters for methane are σ = 3.72 Å and ε = 1.318 kJ/mol;[42] the Lorentz−Berthelot combining rules are used for water−methane interactions. The simulations are performed using the open source code Gromacs.[43−45] Full periodic boundary conditions are applied in all directions. A time-step of 2 fs is used. Short-range interactions are truncated at 1.2 nm and long-range electrostatic interactions are computed using the smooth particle mesh Ewald summation. For the 3 ns simulation run we use Berendsen[46] barostat and thermostat with relaxation time constants τ_p = 0.1 ps and τ_T =

Table 1. Summary of the Conditions in our Study[a]

run #	n_r	N_m	N_w	T (K)	t_N (ns)	x_m
1	2	256	2944	250	37, 53.5	0.08
2	2	256	2944	260	21, 19.6	0.08
3	2	256	2944	275	5, 6	0.08
4	1	768	8832	275	3.5	0.08
5	2	256	2944	285	3.5, 17	0.08
6	1	768	8832	285	15	0.08
7	2	1024	11776	285	11, 17.5	0.08
8	1	1280	14720	285	20	0.08

[a]First column gives the label of the run, second column is the number of runs for the specified conditions (n_r), third coulumn is the number of methane molecules (N_m), fourth column is the number of water molecules (N_w), fifth column is the temperature (T), sixth column are the nucleation times (t_N), and seven column is the methane mole fraction (x_m). The pressure is equal to 50 MPa in all the runs.

0.5 ps, respectively. For the long simulation we use the Nosé–Hoover[47,48] thermostat with a relaxation time of τ_T = 2 ps, whereas the pressure is kept constant by means of the Parrinello–Rahman[49] barostat with a relaxation time of τ_P = 4 ps. The leapfrog algorithm is used for integrating Newton's equation of motion, and rigid water molecule constraints are implemented with the SHAKE algorithm.[50] Our simulations are performed at T = 250, 260, 275, and 285 K. The pressure is kept constant at P = 50 MPa (see Table 1). Our estimation of the melting temperature for sI of methane hydrate at 50 MPa is 304 K as mentioned above.

The methane to water ratio in the crystalline sI of methane hydrates is 1/5.75 which corresponds to a methane mole fraction of x_m = 0.16. By preparing mixtures with different contents of methane we observe that a methane mole fraction up to ∼0.09 remains dissolved in water at P = 50 MPa and T = 285. At a higher methane concentration (x_m = 0.098 with N_m = 320, N_w = 2944), the mixture separates in less than 3 ns into a methane gas phase and an aqueous solution with few dissolved molecules of methane (spinodal decomposition). In a similar way, at T = 290 K, we find that the limit of dissolved methane is less than 0.08 mole fraction. In our study we choose a methane mole fraction of 0.08.

The experimental equilibrium solubility of methane in water at hydrate conditions is $x_m \sim 10^{-3}$.[51,52] A metastable solution above this value may exist and is consistent with thermodynamics. The CPA equation of state reproduces experimental solubility of hydrocarbons and other compounds in water with a high degree of accuracy.[53] The maximum metaestable solubility of methane in water computed by means of the CPA equation of state is $x_m \approx 0.1$ at T = 285 K and P = 50 MPa. This value is in agreement with our estimated value from molecular dynamics simulations.

RESULTS

We observe hydrate formation in all of our simulations. The nucleation time is defined as the time when the sustained

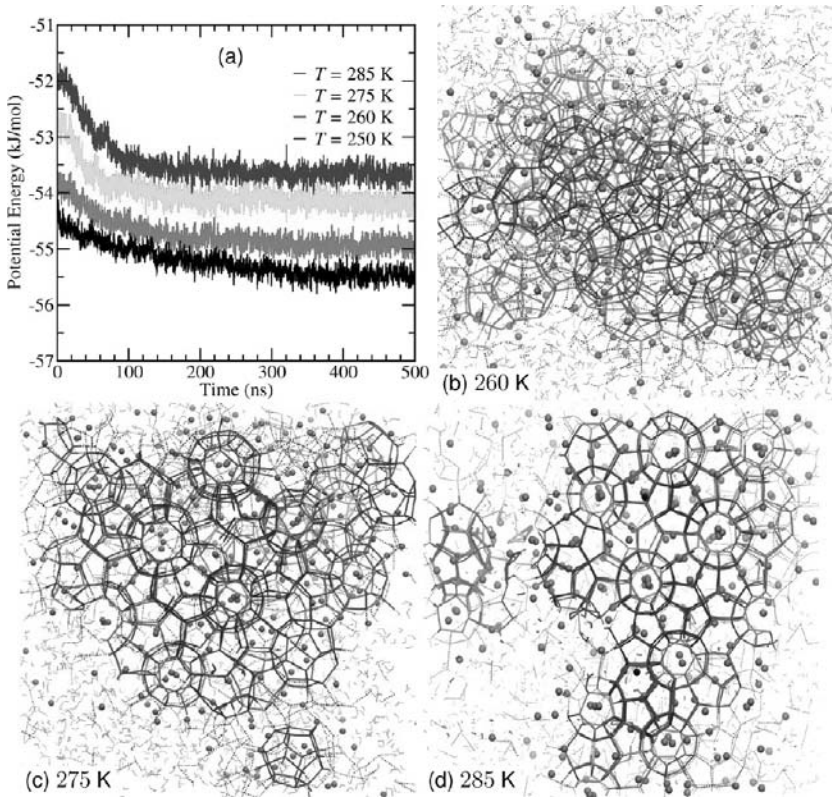

Figure 1. (a) Potential energy of the system during simulation for the small setup (N_m = 256, N_w = 2944) at T = 250 (black line), 260 (red line), 275 (green line), and 285 K (blue line); P = 50 MPa in all cases. Snapshots of the simulation box at the end of the simulation run: (b) T = 260, (c) 275, and (d) 285 K. Water molecules are represented by two light blue lines joining the oxygen–hydrogen centers, whereas methane molecules are represented by red spheres. A color code is used to distinguish different types of cages: red is the small 5^{12}, blue is $5^{12}6^2$, green is $5^{12}6^3$, and gray is $5^{12}6^4$.

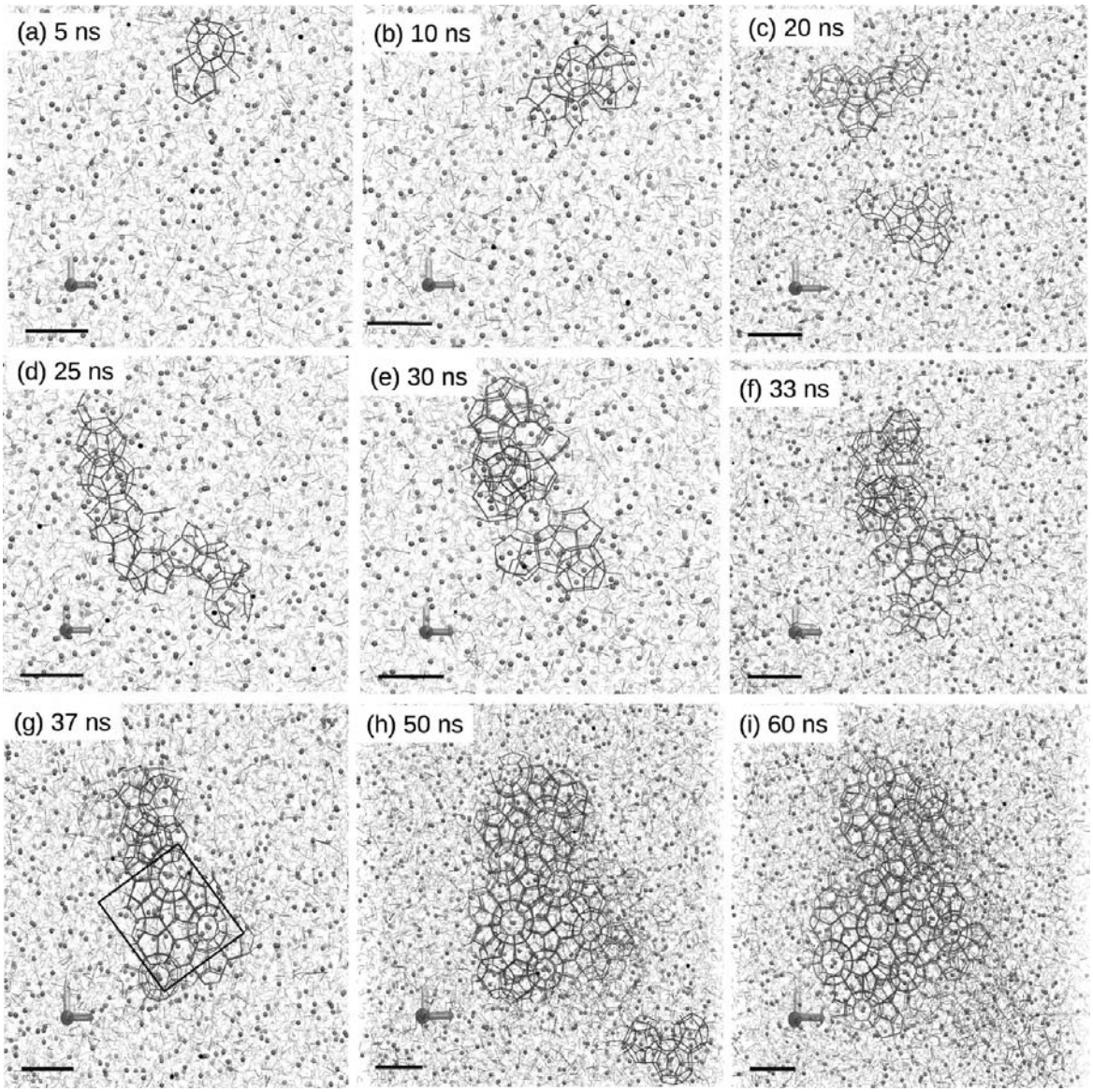

Figure 2. Snapshots of the simulation box at different times showing several stages of nucleation and growth of sI of methane hydrate. Water molecules are represented by two light blue lines joining the oxygen−hydrogen centers whereas methane molecules are represented by red spheres. A hydrogen bond (dotted black lines) is formed between the oxygen from an acceptor water molecule and the hydrogen atom from a donor water molecule when they are within a separation distance of 3 Å and form an angle equal or less than 10° with the donor oxygen. Some of the hydrogen bonds are highlighted with thicker lines to aid visualization. The snapshots are taken from the same angle at different magnifications (see the 10 Å scale bar and coordinate axis at the lower left corner). Simulation conditions are N_w = 11776, N_m = 1024, T = 285 K, and P = 50 MPa.

growth of hydrate structure initiates. In terms of the number of cages produced as a function of time, nucleation time is the latest time when the number of cages is equal to zero. The nucleation times of our simulation runs are reported in the sixth column of Table 1. The nucleation times for 0.08 methane mole fraction are between 3 and 53.5 ns. There is a decreasing trend of the nucleation time associated with temperature between T = 250 and 275 K. At T = 285 K, the nucleation time is higher than at T = 275 K, but some unstable cages form as early as 3 ns. For the highest temperature, some clusters form before t = 5 ns which do not remain stable. The simulations at T = 285 K have nucleation times between 11 and 20 ns, with no clear trend associated with the size of the system. This is consistent with nucleation theory where nucleation time reduces as supersaturation increases.[16] Sarupria and Debenedetti[36] report a nucleation time of several hundreds of nanoseconds for x_m = 0.07 at T = 240 K and P = 20 MPa. At those conditions, we obtain a nucleation time of ∼300 ns, in line with their values.

Figure 1a portrays the potential energy versus simulation time of the methane−water small setup at four different temperatures (runs 1−4 corresponding to temperatures from 250 to 285 K, respectively). In general, the four plots show a decreasing trend toward an asymptotic value as time increases. The system reaches its stationary state faster, while a larger potential energy drop is produced with the increase of temperature. The plots at T = 275 and 285 K have a small shoulder at around t = 50 and 70 ns, respectively. At this point, the systems reach a metastable state from which they escape easily due to their high temperature fluctuations. The potential

energy is always decreasing during the whole simulation run, even if the nucleation time is of several tens of nanoseconds (e.g., at T = 250 K, P = 50 MPa, and x_m = 0.08). This is different from the simulations starting from two-phase systems where periods of constant potential energy are observed and the main drops occur during the dissolution of methane into water and the ordering of the structures.[23,28] In both cases (mixed or separated components), the equilibrium is only reached when the hydrate forms.

In our simulations, a larger energy drop is indicative of the higher order of the structure formed. At T = 250 (not shown) and 260 K (Figure 1b), amorphous clusters form. At T = 275 K (Figure 1c), a more regular structure with some irregular regions is observed, and at T = 285 K (Figure 1d), a much more regular cluster is formed. Similarly, ref 35 reports the continuous increase of temperature results in exothermic formation of H_2S hydrates structures sI, sII, and HS-I. Our results at T = 250 K are qualitatively similar to those obtained by initially having the two components separated by an interface.[22] In the latter, however, the dissolution of methane into water significantly increases the computational time. There is a correlation between the number of cages formed and temperature. We will discuss this point later.

The clusters shown in Figure 1b−d are mostly cages of the type 5^{12}, with 12 pentagonal faces conformed by 20 water molecules (red cages in Figure 1b−d). A larger cage denoted as $5^{12}6^2$ consists of two hexagonal faces and 12 pentagonal faces (blue cages in Figure 1b−d). The unit cell of sI is composed of two 5^{12} and six $5^{12}6^2$ cages.[54] In sI, the $5^{12}6^2$ cages may share hexagonal and pentagonal faces. 5^{12} cages, on the other hand, occupy empty spaces and do not share faces when they are in sI, while they do in sII. The $5^{12}6^4$ cages are specific to sII (gray cages in Figure 1d). The $5^{12}6^3$ cages are metastable (green cages in Figure 1b−d) and have been observed in other studies in methane hydrate nucleation.[22,23] The clusters formed at T = 275 and 285 K exhibit clear traces of sI and sII. Larger systems are selected to form domains of the crystalline phases. Runs 4 and 6 are three times larger, run 7 is four times larger, and run 8 is five times larger (see Table 1). Despite the fact that nucleation is a random process, the general features are similar for different system sizes. Below we present the results for run 7. A comparison among different setups is presented afterward by computing the average number of cages.

In Figure 2 snapshots of the simulation box for one of the simulations of run 7 (N_m = 1024, N_w = 11776 at T = 285 K) at different simulation times are shown. At t = 0 (not shown), a single phase is made of methane molecules in water. No structure is initially observed. At early stages during the simulation, stable pentagonal faces appear and around t = 5 ns the first stable cage forms and the growing of an amorphous cluster initiates (Figure 2a,b). Another amorphous cluster is formed at a different region in the simulation box (Figure 2c). The cages formed so far are of the type 5^{12}; some are not fully developed. At some point both clusters coalesce and form a single larger amorphous cluster (Figure 2d). At the time of coalescence, the cluster extends nearly over the full length of the box. After coalescence, the cluster becomes more compact (Figure 2e). Between t = 30 and 33 ns at the central region of the box (at the region where coalescence takes place), the first traces of sI appear (Figure 2e,f). At the time when the first traces of sI are formed the cluster's longest dimension is around 4.5 nm.

In Figure 2f, the hexagonal faces of a $5^{12}6^2$ cage are shown at the upper corner of the highlighted box. Another cage of the same kind is seen at the central region exhibiting its pentagonal lateral faces while it shares a hexagonal face with an incomplete cage. The cages at the two lowest corners of the red box are of the type 5^{12}, however, they are not conforming sI. These cages are expected to transform in longer times into $5^{12}6^2$ to conform the long-range order of sI. The methane molecules apparently within the cages are actually aligned molecules forming a row, implying that other cages are formed in the z direction. At t = 37 ns, the two $5^{12}6^2$ cages at the center of the box are completely formed and a new row of the same cages is nucleated at the upper left corner of the box. At t = 50 ns, the second row is fully formed and the growth continues. An amorphous cluster is formed at the lower right corner of the simulation box and approaches the larger cluster. At t = 60 ns, sI at the central region of the box is well-defined and the cluster continues growing in all directions. The structure of the cluster at the lower region of box is rather amorphous but shows the formation of many hydrogen bonds. The upper part of the cluster turns progressively more ordered, and at this region, the elements of sII appear afterward (see discussion below).

To quantify our results, we use an algorithm similar to that proposed by Jacobson et al. to classify the cage geometry.[32] We identify cages by looking for oxygen atoms within a distance of 6.1 Å from a central methane molecule. Then we use the connectivity of water molecules and the topology of the rings they form.[55] Two oxygen atoms are connected if they are within a distance of 3.5 Å. We look for all possible pentagonal and hexagonal rings formed by connected oxygen atoms. Oxygen atoms are the vertices of an undirected graph to identify the rings. This procedure is used to identify the 5^{12}, $5^{12}6^2$, $5^{12}6^3$, and $5^{12}6^4$ cages composed of 20, 24, 26, and 28 water molecules, respectively. To determine the number of empty 5^{12} cages we look for complementary half cages constructed from a pentagonal ring surrounded by five connected pentagonal rings. The cages with a methane molecule inside are discarded. We assume cages other than 5^{12} to be filled due to larger size.

Figure 3 shows the evolution of the number (n_c) of different types of cages formed in one of the simulations in run 7. Around $t \approx$ 30 ns the sustained growth of 5^{12} cages initiates.

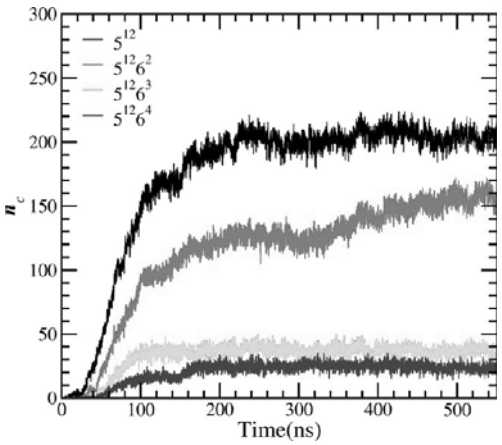

Figure 3. Evolution of cage types during simulation for run 7. The lines shown are coded as follows: black for 5^{12}; red for $5^{12}6^2$; green for $5^{12}6^3$; and blue for $5^{12}6^4$ cages.

Few complete cages are formed before this time. The larger $5^{12}6^2$ cages appear around $t \approx 35$ ns followed by their sustained growth. Their appearance is clearly related to the formation of sI as discussed above. $5^{12}6^3$ and $5^{12}6^4$ cages appear at $t \approx 60$ and 80 ns, respectively. The 5^{12} cage is the most abundant in the entire simulation followed by $5^{12}6^2$. The $5^{12}6^4$ cage, which belongs to sII, is the smallest fraction. The formation is related to the appearance of domains of sII as we will discuss below. The rate of formation of 5^{12} and $5^{12}6^2$ cages is very high before $t \approx 120$ ns and tend to stabilize in the long time. The formation of $5^{12}6^3$ and $5^{12}6^4$ cages is at lower rate than the smaller cages and reach stable values faster. The plots of the number of cages as a function of time for all our simulations are presented in Figure S1 of the Supporting Information. For run 7, empty cages represent about 3% of the total number of 5^{12} cages which is less than 2% of the total number of cages. Later we will have further discussion on the number of empty cages.

The tetrahedral order parameter[56] is defined as $F_3 = \langle \sum_{j=1}^{n_i-1} \sum_{k=j+1}^{n_i} (|\cos \theta_{jik}| \cos \theta_{jik} + 1/9)^2 \rangle$, where n_i is the number of oxygen atoms within a distance of 3.5 Å from the ith atom and θ_{jik} is the angle formed by the oxygen atoms i, j, and k. The four-body order parameter[57,58] is defined as $F_4 = \langle \cos 3\phi \rangle$, where ϕ is the torsion angle of the configuration H−O···O−H formed with the outermost hydrogen atoms of two adjacent water molecules. Averages $\langle ... \rangle$ are computed over the total number of water molecules. F_3 is equal to zero for a tetrahedral network and F_4 is 0.7 for hydrate (for both sI and sII), −0.04 for liquid water, and −0.4 for ice. Figure 4 shows the evolution

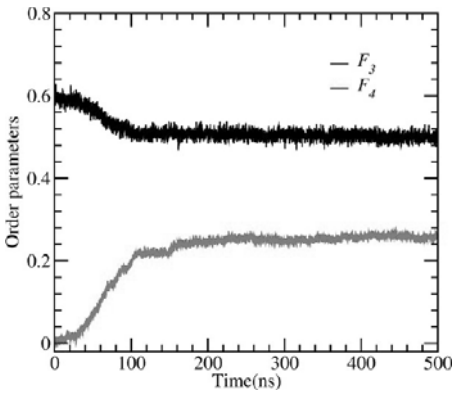

Figure 4. Evolution of the order parameters F_3 (black) and F_4 (red) for run 7 over the course of the simulation.

of both parameters for run 7. At the beginning of the simulations F_4 is around −0.01 and increases monotonically to reach an average value around 0.25. F_3 starts from a value above 0.6 and decreases to an average value of 0.5. The intermediate values of F_3 and F_4 between the liquid and hydrate structure at the end of the simulation is a reflection of the fact that there is a large number of water molecules in liquid state. The plots of the order parameters for all our simulations are in Figure S2 of the Supporting Information.

Figure 5 shows the average number of cages per number of methane molecules n^i/N_m with $i = 1$ for 5^{12}, $i = 2$ for $5^{12}6^2$, $i = 3$ for $5^{12}6^3$, and $i = 4$ for $5^{12}6^4$. Averages are computed over 50 ns of stable potential energy. Some trends are observed in the overall behavior. For example, in systems with the same size (runs 1−3 and 5) the number of $5^{12}6^n$ cages with $n = 2$−4 increases as the temperature increases. Also, the total number of cages n_T increases with temperature (n_T = 57, 58, 87, and

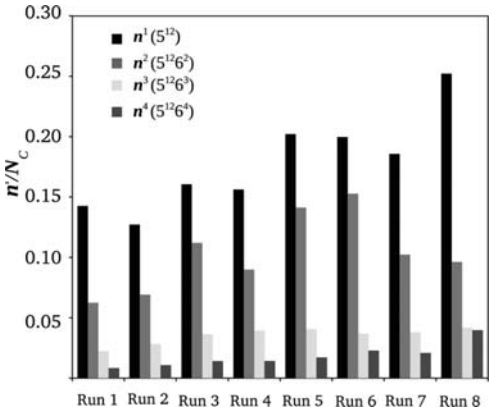

Figure 5. Average number of cages classified by their geometry per methane molecule n^i/N_c with $i = 1, ..., 4$ coded as follows: black for 5^{12} cages ($i = 1$); red for $5^{12}6^2$ cages ($i = 2$); green for the $5^{12}6^3$ cages ($i = 3$); and blue for $5^{12}6^4$ cages ($i = 3$). Averages are computed over the last 50 ns of simulation time.

100 for T = 250, 260, 275, and 285 K, respectively). The more pronounced increase occurs at the two highest temperatures. As we mention above (see discussion of Figure 1), there is a correlation between the number of cages formed and the energy drop. As the system size increases and the temperature is kept at 285 K (runs 4 and 6−8), there is no clear trend, but the overall behavior is random. For the simulations of run 7, the number of 5^{12} and $5^{12}6^2$ cages is very different, whereas the number of $5^{12}6^3$ and $5^{12}6^4$ cages is similar. In general, the relative number of $5^{12}6^3$ cages per methane molecules remains around 0.04 as the system size increases (runs 4 and 6−8). The largest setup (run 8) shows the increase of the relative number of 5^{12} and $5^{12}6^4$ cages in comparison to the smaller systems.

Figure 6 shows the fraction of empty 5^{12} cages n_e/n^1. For the setups of the same size (runs 1−3), a decreasing trend with

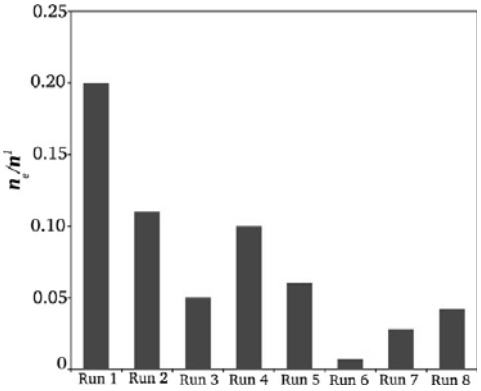

Figure 6. Fraction of empty 5^{12} cages. Averages are computed over the last 50 ns of simulation time.

temperature is observed. At 285 K (run 5), the fraction of empty cages is ∼0.06, slightly higher than for run 3 at T = 275 K. The larger setup at T = 275 K (run 4) has a higher fraction of empty cages (∼0.1). For run 6, a single empty cage is detected that gives a fraction below 0.01. For runs 7 and 8 at T = 285 K, the fraction of empty cages is around 0.04 and 0.03, respectively. The ratio of empty cages with respect to the total number of cages is approximately one-half of the values plotted in Figure 6.

dx.doi.org/10.1021/jp5002012 | J. Phys. Chem. C 2014, 118, 11310−11318

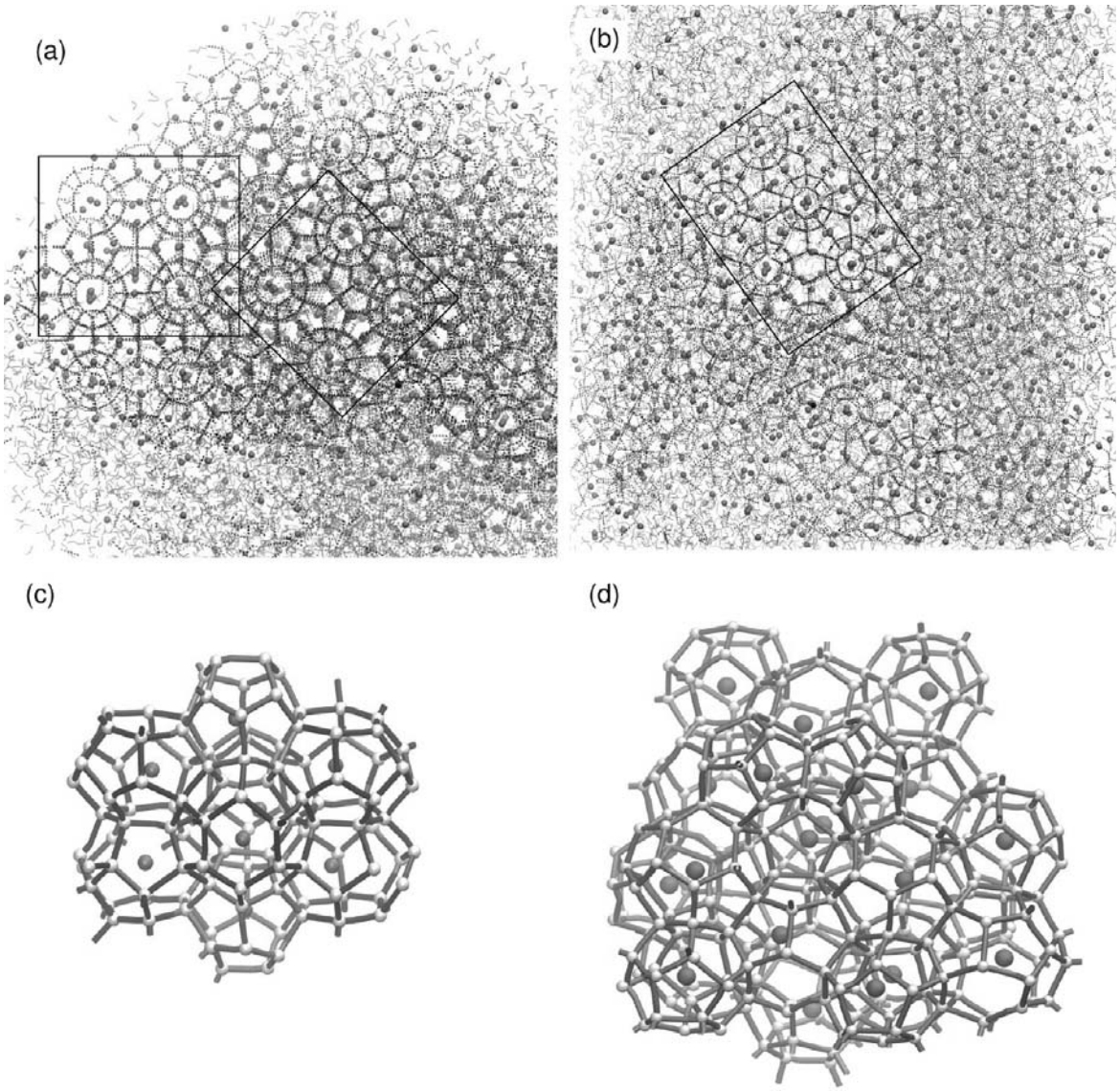

Figure 7. Snapshots of the simulation box at 500 ns of simulation exhibiting domains of sI (a) and sII (b). The snapshots are taken from different angles and the crystalline domains are highlighted by a black box (see Figure 2 for the notation). Extracted portions of sI (c) and sII (d) were obtained from molecular dynamics simulations. Red, blue, and gray colors are used for the 5^{12}, $5^{12}6^2$, and $5^{12}6^4$ cages, respectively. Simulation conditions are N_w = 11776, N_m = 1024, T = 285 K, and P = 50 MPa.

The structures at the end of the simulations consist of sI and sII. Figure 7a,b displays two regions of the simulation box for run 7 at t = 500 ns. Figure 7a exhibits two regions of completely formed sI, whereas Figure 7b shows a region with sII. Figure 7c,d displays two clusters extracted from our simulations of sI and sII, respectively, approximately of the size of unit cells. Coexistence of sI and sII has been observed experimentally as a kinetic state toward the thermodynamically stable sI hydrate structure.[59−61] Other regions of the cluster show domains of aligned 5^{12} cages at the edges or incorporated as defects within sI and similarly observed at very high pressure.[23] This in turn explains the large number of 5^{12} over the other types of cages. Additionally, the sII hydrate contains eight times more 5^{12} cages per unit cell than sI.

A rough estimation of the fraction of sI and sII is obtained by grouping the cages in sI and sII. The $5^{12}6^2$ cages sharing at least one face with another similar cage or with a 5^{12} cage are classified in sI. Similarly, 5^{12} cages are classified in sI if they share a face with a $5^{12}6^2$ cage. The fraction of sI is $\phi_I = n_{sI}/n_T$, where n_{sI} is the number of cages in sI and n_T is the total number of cages of all geometries. In a similar way, the fraction of cages in sII is given as $\phi_{II} = n_{sII}/n_T$, where n_{sII} is the number of cages in sII. The $5^{12}6^4$ cages are in sII if they are next to a similar cage or next to a 5^{12} cages.[54] The results for the runs at T = 285 K are shown in Figure 8. In all runs the fraction of sI is higher than sII. The setups with the same size (run 7) have approximately the same fraction of sII. Interestingly, the largest setup (run 8) contains the largest fraction of sII and the lowest of sI.

An important feature in our simulations is the composition of the mixture. In a real system, a concentration of methane in water of x = 0.08 similar to that in our simulations may be established by bringing water and methane into contact at a very high pressure ($\sim 10^3$ MPa) and high temperature (T = 450

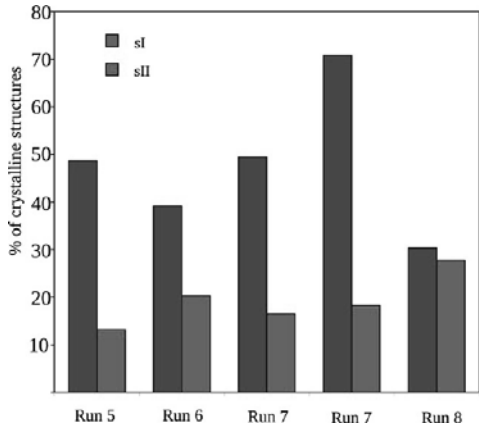

Figure 8. Percentage of cages in sI (blue bars) and sII (red bars) for the different setups at T = 285 K and P = 50 MPa.

K). Then, pressure and temperature are lowered to our simulation conditions (P = 50 MPa and T = 285 K). Degassing does not occur instantaneously, and water and methane remain in a metastable mixture. Note that methane mole fraction in a fully occupied sI of methane hydrate is x_m = 0.16. Our simulations are carried out at half of that concentration and show that only a few nanoseconds are needed to form hydrates at these conditions. This result is advantageous from the computational point of view. At the beginning of this section we point out that a mixture with a concentration of methane higher than the equilibrium concentration may exist. Our molecular dynamics simulations and a well established equation of state support it.

CONCLUSIONS

We have selected a supersaturated methane−water mixture in our hydrate molecular simulation. This allowed us simulating homogeneous methane hydrate nucleation of large systems in short computational times at moderate conditions (T = 285 K at P = 50 MPa).[54] Different from many other studies there is no interface initially[19−24] nor pre-existing hydrate structures[33,34,38,39] in our work. The distinctive feature of our study is the formation of crystalline domains of sI and sII at moderate temperatures and moderate pressure. Other authors have observed formation of sI at high pressure and low temperature[23] or by having dynamic variations of temperature.[24,34,35] We find that a larger potential energy drop is observed as the temperature increases which in turn is correlated with a higher order of the structures formed. The hydrate nucleation initiates with the formation of an amorphous cluster from which the crystalline domains originate. We observe complete domains of methane hydrate sI and sII, in agreement with experiments.[59−61] In all cases, the fraction of sI is higher than sII. Only in the largest simulated setup the factions of both structures are comparable. The driving force for nucleation is provided by the high concentration of methane in water.[18] The high mobility of water and methane molecules at moderate subcooling reduce nucleation times. We observe the whole two-step nucleation process from the initial formation of an amorphous cluster to the formation of the crystalline structures.[24,34] Our study in homogeneous hydrate nucleation combines a moderate pressure and temperatures above the freezing point of water, which are the conditions for many applications. These conditions are required in future kinetic and antiagglomeration studies by surfactants.

ASSOCIATED CONTENT

Supporting Information

Figures S1 and S2. This material is available free of charge via the Internet at http://pubs.acs.org.

AUTHOR INFORMATION

Corresponding Author

*E-mail: abbas.firoozabadi@yale.edu. Phone: +1 (650)326-9172. Fax: +1 (650) 472-9285.

Notes

The authors declare no competing financial interest.

ACKNOWLEDGMENTS

We thank the member companies of the Reservoir Engineering Research Institute (RERI) for their financial support.

REFERENCES

(1) Englezos, P. Clathrate Hydrates. *Ind. Eng. Chem. Res.* **1993**, *32*, 1251−1274.
(2) Koh, C. A. Towards a Fundamental Understanding of Natural Gas Hydrates. *Chem. Soc. Rev.* **2002**, *31*, 157−167.
(3) Gao, S.; House, W.; Chapman, W. G. NMR/MRI Study of Clathrate Hydrate Mechanisms. *J. Phys. Chem. B* **2005**, *109*, 19090−19093.
(4) Park, Y.; Kim, D.-Y.; Lee, J.-W.; Huh, D.-G.; Park, K.-P.; Lee, J.; Lee, H. Sequestering Carbon Dioxide into Complex Structures of Naturally Occurring Gas Hydrates. *Proc. Natl. Acad. Sci. U.S.A.* **2006**, *103*, 12690−12694.
(5) Chatti, I.; Delahaye, A.; Fournaison, L.; Petitet, J.-P. Benefits and Drawbacks of Clathrate Hydrates: A Review of Their Areas of Interest. *Energy Convers. Manage.* **2005**, *46*, 1333−1343.
(6) Glasby, G. Potential Impact on Climate of the Exploitation of Methane Hydrate Deposits Offshore. *Mar. Pet. Geol.* **2003**, *20*, 163−175.
(7) Florusse, L. J.; Peters, C. J.; Schoonman, J.; Hester, K. C.; Koh, C. A.; Dec, S. F.; Marsh, K. N.; Sloan, E. D. Stable Low−Pressure Hydrogen Clusters Stored in a Binary Clathrate Hydrate. *Science* **2004**, *306*, 469−471.
(8) Mao, W. L.; Mao, H.-K.; Goncharov, A. F.; Struzhkin, V. V.; Guo, Q.; Hu, J.; Shu, J.; Hemley, R. J.; Somayazulu, M.; Zhao, Y. Hydrogen Clusters in Clathrate Hydrate. *Science* **2002**, *297*, 2247−2249.
(9) Reagan, M. T.; Moridis, G. J. Global Climate and the Response of Oceanic Hydrate Accumulations. *Meth. Hyd. Newslett.* **2010**, *10*, 9−12.
(10) Koh, C. A.; Sloan, E. D.; Sum, A. K.; Wu, D. T. Fundamentals and Applications of Gas Hydrates. *Annu. Rev. Chem. Biol. Eng.* **2011**, *27*, 237−257.
(11) Collett, T. S.; Kuuskraa, V. A. Hydrates Contain Vast Store of World Gas Resources. *Oil Gas J.* **1998**, *96*, 90−95.
(12) Lee, S.-Y.; Holder, G. D. Methane Hydrates Potential as a Future Energy Source. *Fuel Process. Technol.* **2001**, *71*, 181−186.
(13) Sloan, E. D. Fundamental Principles and Applications of Natural Gas Hydrates. *Nature* **2003**, *426*, 353−363.
(14) Bagirov, E.; Lerche, I. Hydrates Represent Gas Source, Drilling Hazard. *Oil Gas J.* **1997**, *95*, 99−104.
(15) Graham, B.; Reilli, W. K.; Beinecke, F.; Boesch, D. F.; Garcia, T. D.; Murray, C. A.; Ulmer, F. Deep Water: The Gulf Oil Disaster and the Future of Offshore Drilling. *Report to the President*; 2011.
(16) Yoreo, J. J. D.; Vekilov, P. In *Biomineralization*; Dove, P. M., Yoreo, J. J. D., Weiner, S., Eds.; Mineralogical Society of America: Washington, DC, 2003; Vol. *54*, pp 57−93.
(17) Abraham, F. F. *Homogeneous Nucleation Theory*; Academic Press: New York, 1974.

(18) Kashchiev, D.; Firoozabadi, A. Driving Force for Crystallization of Gas Hydrates. *J. Cryst. Growth* **2002**, *241*, 220−230.
(19) Moon, C.; Taylor, P. C.; Rodger, P. M. Molecular Dynamics Study of Gas Hydrate Formation. *J. Am. Chem. Soc.* **2003**, *125*, 4706−4707.
(20) Zhang, J.; Hawtin, R. W.; Yang, Y.; Nakagava, E.; Rivero, M.; Choi, S. K.; Rodger, P. M. Molecular Dynamics Study of Methane Hydrate Formation at a Water/Methane Interface. *J. Phys. Chem. B* **2008**, *112*, 10608−10618.
(21) Hawtin, R. W.; Quigley, D.; Rodger, P. M. Gas Hydrate Nucleation and Cage Formation at a Water/Methane Interface. *Phys. Chem. Chem. Phys.* **2008**, *10*, 4853−4864.
(22) Walsh, M. R.; Koh, C. A.; Sloan, E. D.; Sum, A. K.; Wu, D. T. Microsecond Simulations of Spontaneous Methane Hydrate Nucleation and Growth. *Science* **2009**, *326*, 1095−1098.
(23) Walsh, M. R.; Rainey, J. D.; Lafond, P. G.; Park, D.-H.; Beckham, G. T.; Jones, M. D.; Lee, K.-H.; Koh, C. A.; Sloan, E. D.; Wu, D. T.; Sum, A. K. The Cages, Dynamics, and Structuring of Incipient Methane Clathrate Hydrates. *Phys. Chem. Chem. Phys.* **2011**, *13*, 19951−19959.
(24) Jacobson, L. C.; Hujo, W.; Molinero, V. Amorphous Precursors in the Nucleation of Clathrate Hydrates. *J. Am. Chem. Soc.* **2010**, *132*, 11806−11811.
(25) Jacobson, L. C.; Hujo, W.; Molinero, V. Nucleation Pathways of Clathrate Hydrates: Effect of Guest Size and Solubility. *J. Phys. Chem. B* **2010**, *132*, 13796−13807.
(26) Liang, S.; Kusalik, P. G. Exploring Nucleation of H_2S Hydrates. *Chem. Sci.* **2011**, *2*, 1286−1292.
(27) Ripmeester, J. A.; Alavi, S. Molecular Simulations of Methane Hydrate Nucleation. *ChemPhysChem* **2010**, *11*, 978−980.
(28) Walsh, M. R.; Beckham, G. T.; Koh, C. A.; Sloan, E. D.; Wu, D. T.; Sum, A. K. Methane Hydrate Nucleation Rates from Molecular Dynamics Simulations: Effects of Aqueous Methane Concentration, Interfacial Curvature, and System Size. *J. Phys. Chem. C* **2011**, *115*, 21241−21248.
(29) Guo, G.-J.; Rodger, P. M. Solubility of Aqueous Methane Under Metastable Conditions. *J. Phys. Chem. B* **2013**, *117*, 6498−6504.
(30) Conde, M. R.; Vega, C. Determining the Three-Phase Coexistence Line in Methane Hydrates Using Computer Simulations. *J. Chem. Phys.* **2010**, *133*, 064507−1−12.
(31) Guo, G.-J.; Zhang, Y.-G.; Wu, C.-H. Can the Dodecahedral Water Cluster Naturally Form in Methane Aqueous Solutions? A Molecular Dynamics Study on the Hydrate Nucleation Mechanisms. *J. Chem. Phys.* **2008**, *128*, 194504−1−8.
(32) Jacobson, L. C.; Hujo, W.; Molinero, V. Thermodynamic Stability and Growth of Guest-Free Clathrate Hydrates. *J. Phys. Chem. B* **2009**, *113*, 10298−10307.
(33) Vatamanu, J.; Kusalik, P. G. Unusual Crystalline and Polycrystalline Structures in Methane Hydrates. *J. Am. Chem. Soc.* **2006**, *128*, 15588−15589.
(34) Vatamanu, J.; Kusalik, P. G. Observation of Two-Step Nucleation in Methane Hydrates. *Phys. Chem. Chem. Phys.* **2010**, *12*, 15065−15072.
(35) Liang, S.; Kusalik, P. G. Nucleation of Gas Hydrates within Constant Energy Systems. *J. Phys. Chem. B* **2013**, *117*, 1403−1410.
(36) Sarupria, S.; Debenedetti, P. G. Homogeneous Nucleation of Methane Hydrate in Microsecond Molecular Dynamics Simulations. *J. Phys. Chem. Lett.* **2012**, *3*, 2942−2947.
(37) Vatamanu, J.; Kusalik, P. G. Molecular Insights into the Heterogeneous Crystal Growth of sI Methane Hydrate. *J. Phys. Chem. B* **2006**, *110*, 15896−15904.
(38) Tung, Y.-T.; Chen, L.-J.; Chen, Y.-P.; Lin, S.-T. The Growth of Structure I Methane Hydrate from Molecular Dynamics Simulations. *J. Phys. Chem. B* **2010**, *114*, 10804−10813.
(39) Jacobson, L. C.; Molinero, V. Can Amorphous Nuclei Grow Crystalline Clathrates? The Size and Crystallinity of Critical Clathrate Nuclei. *J. Am. Chem. Soc.* **2011**, *133*, 6458−6463.
(40) The melting temperature is determined following the method of ref 30 with 1 K of accuracy. We used a sI methane hydrate crystal slab made of 3 × 3 × 5 unit cells (2070 water molecules and 360 methane molecules) next to an aqueous phase (1000 water molecules with 100 methane molecules dissolved). A methane gas phase (260 molecules) is located next to the aqueous solution.
(41) Abascal, J. L. F.; Sanz, E.; García Fernández, R.; Vega, C. A Potential Model for the Study of Ices and Amorphous Water: TIP4P/Ice. *J. Chem. Phys.* **2005**, *122*, 234511−1−9.
(42) Calero, S.; Dubbeldam, D.; Krishna, R.; Smit, B.; Vlugt, T. J. H.; Denayer, J. F. M.; Martens, J.; Maesen, T. L. M. Understanding the Role of Sodium During Adsorption: A Force Field for Alkanes in Sodium-Exchanged Faujasites. *J. Am. Chem. Soc.* **2004**, *126*, 11377−11386.
(43) Berendsen, H.; Spoel, D. V. D.; Drunen, R. V. Gromacs: A Message-Passing Parallel Molecular Dynamics Implementation. *Comput. Phys. Commun.* **1995**, *91*, 43−56.
(44) Spoel, D. V. D.; Lindahl, E.; Hess, B.; Groenhof, G.; Mark, A. E.; Berendsen, H. J. C. GROMACS: Fast, Flexible, and Free. *J. Comput. Chem.* **2005**, *26*, 1701−1718.
(45) Hess, B.; Kuttner, C.; van der Spoel, D.; Lindahl, E. GROMACS 4: Algorithms for Highly Efficient, Load-Balanced, and Scalable Molecular Simulation. *J. Chem. Theory Comput.* **2008**, *4*, 435−447.
(46) Berendsen, H. J. C.; Postma, J. P. M.; van Gunsteren, W. F.; Di Nola, A.; Haak, J. R. Molecular-Dynamics with Coupling to an External Bath. *J. Chem. Phys.* **1984**, *81*, 3684−3690.
(47) Nose, S. A Unified Formulation of the Constant Temperature Molecular-Dynamics Methods. *J. Chem. Phys.* **1984**, *81*, 511−519.
(48) Hoover, W. G. Canonical Dynamics: Equilibrium Phase-Space Distributions. *Phys. Rev. A* **1985**, *31*, 1695−1697.
(49) Parrinello, M.; Rahman, A. Crystal Structure and Pair Potentials: A Molecular-Dynamics Study. *Phys. Rev. Lett.* **1980**, *45*, 1196−1199.
(50) Ryckaert, J. P.; Ciccotti, G.; Berendsen, H. J. C. Numerical Integration of the Cartesian Equations of Motion of a System with Constraints: Molecular Dynamics of *n*-Alkanes. *J. Comput. Phys.* **1977**, *23*, 327−341.
(51) Kim, Y. S.; Ryu, S. K.; Yang, S. O.; Lee, C. S. Liquid Water−Hydrate Equilibrium Measurements and Unified Predictions of Hydrate-Containing Phase Equilibria for Methane, Ethane, Propane, and Their Mixtures. *Ind. Eng. Chem. Res.* **2003**, *42*, 2409−2414.
(52) Servio, P.; Englezos, P. Measurement of Dissolved Methane in Water in Equilibrium with Its Hydrate. *J. Chem. Eng. Data* **2002**, *47*, 87−90.
(53) Li, Z.; Firoozabadi, A. Cubic-Plus-Association (CPA) Equation of State for Water-Containing Mixtures: Is "Cross Association" Necessary? *AIChE J.* **2009**, *55*, 1803.
(54) Sloan, E. D.; Koh, C. A. *Clathrate Hydrates of Natural Gases*; CRC Press: Boca Raton, FL, 2008.
(55) Matsumoto, M.; Baba, A.; Ohmine, I. Topological Building Blocks of Hydrogen Bond Network in Water. *J. Chem. Phys.* **2007**, *127*, 134504−1−9.
(56) Baez, L.; Clancy, P. Computer Simulation of the Crystal Growth and Dissolution of Natural Gas Hydrates. *Ann. N.Y. Acad. Sci.* **1994**, *715*, 177−186.
(57) Rodger, P. M.; Forester, T. R.; Smith, W. Simulations of the Methane Hydrate/Methane Gas Interface Near Hydrate Forming Conditions. *Fluid Phase Equilib.* **1996**, *116*, 326−332.
(58) Moon, C.; Hawtin, R. W.; Rodger, P. M. Nucleation and Control of Clathrate Hydrates: Insights From Simulation. *Faraday Discuss.* **2007**, *136*, 367−382 and discussion 395−407..
(59) Schicks, J. M.; Ripmeester, J. A. The Coexistence of Two Different Methane Hydrate Phases under Moderate Pressure and Temperature Conditions: Kinetic versus Thermodynamic Products. *Angew. Chem., Int. Ed.* **2004**, *43*, 3310−3313.
(60) Fleyfel, F.; Devlin, J. P. Carbon Dioxide Clathrate Hydrate Epitaxial Growth: Spectroscopic Evidence for Formation of the Simple type-II Carbon Dioxide Hydrate. *J. Phys. Chem.* **1991**, *95*, 3811−3815.
(61) Staykova, D. K.; Kuhs, W. F.; Salamatin, A.; Hansen, T. Formation of Porous Gas Hydrates from Ice Powders: Diffraction Experiments and Multistage Model. *J. Phys. Chem. B* **2003**, *107*, 10299−10311.